Biophysical Chemistry 18 (1983) 165–179
Elsevier

BPC 00788

REPULSIVE STABILIZATION IN BLACK LIPID MEMBRANES

A HYDRODYNAMIC MODEL

D. GALLEZ

Service de Chimie Physique II, Universite Libre de Bruxelles CP 231, 1050 Brussels, Belgium

Received 22nd December 1982
Revised manuscript received 7th April 1983
Accepted 14th April 1983

Key words: Black lipid membrane; Linear stability analysis; Steric repulsion

A linear stability analysis is performed for a black lipid membrane. The hydrodynamic model consists of a viscous hydrocarbon film sandwiched between two aqueous phases. Attractive forces (van der Waals and electrical) and repulsive forces (steric) are expressed as body forces in the equations of fluid motion in the three phases. The steric repulsion due to overlap of the hydrocarbon chains of the lipids at small film thicknesses is described via an exponentially decaying interaction potential. The dispersion equation displays two modes of vibrations: the bending mode with the two film surfaces transversely in phase, and the squeezing mode with the two surfaces 180° out of phase. For symmetrical films, these two modes are uncoupled, and the squeezing mode (with thickness variations) is stabilized by the repulsive interactions. For nonsymmetrical films (different surface tensions, surface charges, etc.), these two modes are coupled and the asymmetry induces a shift of the marginal stability curve to shorter wavelengths.

1. Introduction

The majority of the studies previously performed on thin fluid film stability were mainly devoted to thin soap films [1–3]. Recently, the experimental and theoretical interest has shifted towards investigating more closely the static [4a–4c] and dynamic [5,6] properties of hydrocarbon films. This new interest is partly motivated by the biological relevance of hydrocarbon films: a cell membrane, for example, is now described as a fluid mosaic of lipids and proteins [7] with a matrix essentially formed by a special hydrocarbon film, the lipid bilayer. This lipid bilayer is often simulated by 'model membranes', i.e., lipid films in a colored or black state. Previous studies were devoted to the dynamic stability analysis of the biological viscoelastic membrane itself [10] or of the colored films [6,8,9]. The goal of this paper is to focus on the stability of black lipid films, where new repulsive forces occur.

The balance of forces is very different in soap films and lipid films. The soap film is an aqueous phase sandwiched between two gaseous bulk phases and stabilized by surfactants. If the surfactants are charged, the two double layers develop inside the film and the overlap of these diffuse layers produces repulsive forces which stabilize the film, by counteracting the attractive van der Waals forces. The lipid film, conversely, is a hydrocarbon phase sandwiched between two aqueous phase. If the lipids are charged, the double layers extend outside the film. The repulsive stabilization must be provided by other forces, of steric origin, due to the overlap of the hydrocarbon chains at very small film thicknesses.

Experimentally, lipid films are formed [4a–4c] by introducing a small amount of lipid solution

onto the opening of a hydrophobic support immersed in an aqueous solution. First the film appears colored (fig. 1a), implying a film thickness of the order of 0.1–1 μm. Its bulk phase is composed of solvent and the hydrophobic part of the lipid molecules, while the polar or ionic head groups face the external solutions. Under suitable conditions, the colored films begins to drain while color bands indicate varying thicknesses across a film. The bands increase in breadth and width until finally the appearance of 'black spots' signals the beginning of formation of the black film. In the state of thinning, two simultaneous processes [4a–4c] are relevant for the lifetime of the film: (i) gradual drainage by border suction, (ii) growth of film thickness fluctuations; the latter process is the subject of this paper. In the black state, the chain ends interact with each other (fig. 1a) for a bilayer thickness of about 60 Å.

A linear stability analysis was previously performed for colored lipid films [9]: the lipid phase was described as a pure viscous (Newtonian) fluid where 'body forces' are operating: van der Waals attractive forces, and electrical forces due to equal surface charges or the presence of an applied potential. The conclusion was that the mode corresponding to thickness variations (called the squeezing mode, SQ) is always unstable, with a lifetime from a few minutes to several hours, according to the electrical parameters. This prediction is in good agreement with experimental observations [11]. The bending mode, BE, corresponding to fluctuations at constant thickness, is stable for positive film tension.

In the present paper, we performed the same stability analysis for black films. This theory on such sterically stabilized films is, to our knowledge, the first theoretical attempt to describe their hydrodynamics. A recent paper [12] also deals with thickness fluctuations in black lipid membranes, but using an energy method. The authors predict a 'root mean square' amplitude and a 'mean increase in area' for long wavelengths compared to film thickness, by assuming equipartition of energy. Their main conclusion is that the black membrane configuration is flat and that the thickness fluctuations are small in amplitude. In our analysis, this would correspond to a stable SQ mode. Small wavy perturbations [13] are also considered as the main source of the difference in thickness, as measured by the capacitance method or light-reflectance method. These two studies [12,13] suppose that a wavy deviation of planarity with 'swelling and indentation' of the bilayer is plausible: an SQ mode may thus be described, even in the case of a black lipid membrane (bilayer).

Two different approaches for the repulsive interactions where simultaneously developed in a linear stability analysis: an 'order parameter' approach [19] and the 'repulsive body force' approach described here. Furthermore, we will discuss the role of a coupling between the BE and SQ modes, due to the asymmetry, which has not been done before.

In detail, in section 2 we introduce the hydrodynamic model, state the equations of motion and perform the linear stability analysis leading to a general dispersion equation. The repulsive forces deriving from an exponentially decaying interaction potential are described in section 3 and the electrical forces in section 4, for a fast and a slow regime. The results are discussed in section 5, with respect to the role of the repulsive stabilization and of the asymmetry.

2. Hydrodynamic model

The model system adopted consists of a nonthinning, planar, black lipid film (LF) (phase 2) bounded by two semi-infinite aqueous phases (1 and 3) (see fig. 1a).

The hydrocarbon core of the lipid bilayer is considered as bulk liquid hydrocarbon composed of a mixture of oleoyl chains and appropriate solvent. Anisotropy in the hydrocarbon is ignored. Even in hydrocarbon crystals this film structure more closely resembles a liquid than a crystal [11]. For the colored film, the isotropic description of the film is clearly appropriate, since lipid molecules are isotropically dissolved in the bulk of the film. For the black films, this assumption must be assessed with caution: in fact, the lipid molecules constituting the bilayer are amphiphiles and their polar head groups (hydrophilic part) will be

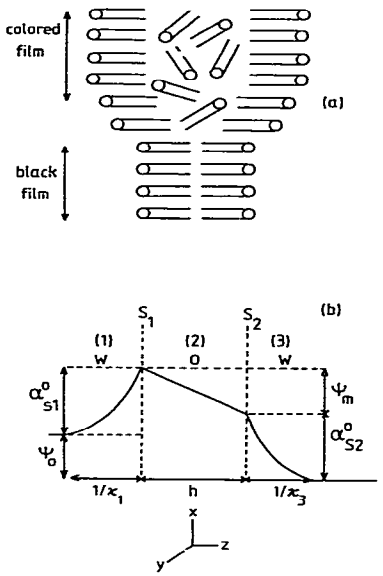

Fig. 1. (a) Formation of black lipid films. The colored film (0.1–1 μm) consists of a bulk lipid solution sandwiched between two layers of surface-adsorbed lipids. In the black film (≈ 60 Å) the two adjacent surfactant layers repel each other sterically. (b) General potential distribution for an asymmetric lipid bilayer. α^0_s, surface potential; ψ_0, applied potential; ψ_m, transmembrane potential; h, membrane width; κ, inverse Debye screening lengths.

arrayed at the two surfaces, facing the aqueous faces (this description takes into account a kind of anisotropy in that sense). However, we suppose here that the hydrophobic parts of the lipid chains are in a 'disordered' state, rendering the hydrocarbon film more 'liquid' than 'solid'. As compared to colored LF (thickness $\approx 10^3$ Å) in which there is no interaction between the two lipid monolayers, these lipid monolayers begin to interact directly with each other in black LF (fig. 1a). Moreover, as the black film width is essentially twice the length of a single lipid molecule, it is problematic to divide the film phase into bulk and surface properties: different parts of the same lipid molecule belong to the surface and to the bulk of the film. However, it is justifiable to identifying the headgroup region with the surface phase and the hydrocarbon chains with the bulk phase, since the head group has a typical width of 3–4 Å as compared to the total film width. The head group regions are thus modelled as two-dimensional surface phases with intrinsic rheology; the surface properties (surface tension, elasticity, coverage, viscosity, etc.) are assumed to be different at the two surfaces, since the two monolayers forming the black LF may be different (asymmetric membranes).

If the film is charged, electrical double layers extend outside in the external aqueous phases. Here, also the surface charges, or the ionic environment, may be different on the two sides of the membrane. The two surface potentials are, respectively, α^0_{s1} and α^0_{s2}. If a potential difference ψ_0 is applied to the membrane (via suitable electrodes and an outside potential source) the 'transmembrane potential' is $\psi_m = \psi_0 + \alpha^0_{s1} - \alpha^0_{s2}$. Inside the film, the potential drop ψ_m is essentially linear due to the low dielectric constant of the lipids (fig. 1b). Film phase 2 is described as a Newtonian incompressible viscous fluid, with a shear viscosity μ_2 and density ρ_2. This is quite a good rheological description for liquid hydrocarbons [9]. 'Incompressibility' here means that, if the film is compressed by an applied potential, for instance, fluid 2 will be 'squeezed out', into the plateau border. The film itself is an 'open' system, in contact with two 'reservoirs', the plateau borders. If fluid 2 is incompressible, the total fluid volume (film + reservoirs) is constant. Other authors [12] describe this situation as 'compressible', which is, in our opinion, a misunderstanding of the notion of incompressibility. Aqueous phases 1 and 3 are also described as Newtonian incompressible fluids with viscosity $\mu_1 = \mu_3$ and density $\rho_1 = \rho_3$. The state of motion in each bulk phase is given by the Navier-Stokes equation

$$\rho \frac{\mathrm{d}}{\mathrm{d}t}\bar{v} = -\bar{\nabla}p + \mu\nabla^2\bar{v} + \bar{F}_E + \bar{F}_V + \bar{F}_R \qquad (1)$$

together with the incompressibility condition $\bar{\nabla}\cdot\bar{v} = 0$ and with

$$\left.\begin{aligned} \bar{F}_E &= \bar{\nabla}\cdot\bar{\bar{T}} \\ \bar{F}_V &= -\rho\bar{\nabla}W_V \\ \bar{F}_R &= -\rho\bar{\nabla}W_R. \end{aligned}\right\} \qquad (2)$$

Here ρ and μ are the uniform mass density and

viscosity, respectively, and $\bar{v}$ the velocity of the phase under consideration. p represents the hydrostatic pressure. The electrical force $\bar{F}_E$, van der Waals force $\bar{F}_V$ and repulsive force $\bar{F}_R$ are introduced as body forces in eq. 1.

The Maxwell tensor is:

$$\bar{\bar{T}} = \frac{1}{4\pi}\left(\epsilon \bar{E}\bar{E} - \tfrac{1}{2}E^2\bar{\bar{I}}\right) \tag{3}$$

with ϵ the dielectric constant, $\bar{E}$ the electric field and $\bar{\bar{I}}$ the unit tensor. $\bar{E}$ is obtained from the electrostatic equations, with the equilibrium Boltzmann distribution, for small potentials (≤ 25 mV) [6].

The van der Waals potential is given by:

$$W_V(\bar{r}) = \int w_V(|\bar{r} - \bar{r}'|)\rho(\bar{r}')\mathrm{d}\bar{r}' \tag{4}$$

where $w_V(|\bar{r} - \bar{r}'|)$ is the long-range part of the two-body potential, asymptotically given by [1]:

$$w_V(|\bar{r} - \bar{r}'|) = -\frac{A}{|\bar{r} - \bar{r}'|^6} \tag{5}$$

where A is the London constant.

The steric repulsive potential W_R describes repulsive interactions at medium range (short-range forces are expressed in the hydrostatic pressure), between the long hydrocarbon chains of the lipids. This potential is determined by a point-point interaction function $w_R(|\bar{r} - \bar{r}'|)$ (the explicit form of this potential is described in the next section) and by the density ρ of the respective phases, so that:

$$W_R(\bar{r}) = \int w_R(|\bar{r} - \bar{r}'|)\rho(\bar{r}')\mathrm{d}\bar{r}'. \tag{6}$$

As for the van der Waals forces, the repulsive forces F_R deriving from this potential are continuous at the two surfaces, so that they can be integrated. Furthermore, we define a 'cut-off' which excludes interactions at very small distances, i.e. $w_R(0) = 0$.

Starting from the plane reference state of the system at rest, we perform a normal mode analysis [14]. Each quantity G is expressed in Fourier components as

$$\delta G(\bar{r}, t) = \delta G(z)\exp(ik_x x + ik_y y)\exp(wt) \tag{8}$$

where $k = (k_x^2 + k_y^2)^{1/2}$ is the wave number (for the geometry see fig. 1b) and $w = w_R + iw_I$ the complex frequency of the perturbation.

The integration constants of the general solution in the bulk phases are fixed via the following boundary conditions (they are similar to those in refs. 6, 8 and 9):

(i) Continuity of velocity.

(ii) Transversal momentum T balance, in which normal surface acceleration and capillary Laplace force (involving surface tension) are balanced by the normal stress due to the action of the bulk forces on the surfaces.

(iii) Longitudinal momentum L balance in which the surface forces due to acceleration, surface viscosity (dissipation) and surface elasticity (local change of surface tension) are balanced by the tangential stress due to the adjoining bulk phases.

(iv) (Dis)Continuity of electrical (field) potential.

A general surface mass and surface charge balance is used, involving surface convection, surface diffusion and adsorption-desorption from the bulk. Two limiting cases will be considered: the 'fast regime' where the convection is fast compared to the two other processes, and the 'slow regime' where the convection is slow and the regime is governed by diffusion and adsorption-desorption.

A general dispersion relation $w = f(k)$ is obtained. This relation is expressed by a 4×4 determinant.

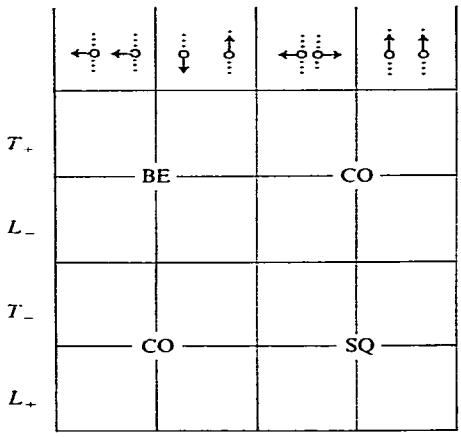

$$= 0 \tag{9}$$

The 2×2 BE mode (fig. 2) couples velocity fields in which the normal displacements are in

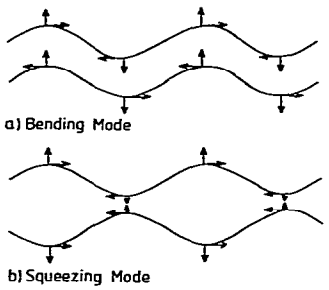

Fig. 2. The two modes of vibration for symmetrical systems: (a) The bending mode (BE) with in-phase transversed displacements. (b) The squeezing mode (SQ) with 180° out-of phase transverse displacements.

phase while the tangential ones are out of phase. For the 2×2 SQ mode, the normal displacements are 180°C out of phase and the tangential ones are in phase. The coupling term CO is due to the mechanical or electrical asymmetry of the film. For completely symmetric systems (same surface tension, elasticity, coverage) and for the following electrical profiles: (1) equal surface charges and zero applied field, (2) external applied field and no surface charges, the two modes BE and SQ are decoupled, and their stability can be analysed separately [6].

However, in the general case of asymmetric membranes treated here, the two modes are coupled. The second and fourth lines of the matrix (eq. 9), respectively, are obtained by subtracting and adding the longitudinal momentum L at the two surfaces S_1 and S_2, and the first and third lines by adding and subtracting the transversal momentum T.

3. The repulsive steric contribution

In this section, we derive an explicit expression for the interaction potential $w_R(|\bar{r} - \bar{r}'|)$ and introduce it in the stability analysis.

Steric stabilization is a general phenomenon which occurs not only in stabilization of colloidal particles by nonionic molecules, in polymer melts [15], but also in stabilization of thin dielectric films (as an example, lipid bilayers that contain few or no solvent molecules). In contrast to aqueous films, which are stabilized by overlap of the electrical double layers inside the film, thin dielectric films are stabilized by overlap of the long hydrocarbon chains. Experiments suggest that two separate regions of close approach must be distinguished [15]: the interpenetration domain (characterized by a thickness of between one and two contour lengths of the stabilizer chains) and the compression domain which is entered on even closer approach. Stabilization of lipid films is referred to the first domain. This justifies the model adopted, in which the film (phase 2) is described as an incompressible fluid with some body forces, attractive and repulsive.

The nature of the repulsive force, or of the related interaction free energy, has been discussed by several authors [16]. The Helmholtz free energy change [11] of the system as the film becomes thinner is, for unit area of the film:

$$\Delta A = A - A_\infty = (\sigma_F - 2\sigma_0) \tag{10}$$

where σ_F is the film tension and σ_0 the interfacial tension of the interfaces between the equilibrium bulk phases. For a system in which adsorption equilibrium with the bulk phases is maintained, this term is calculable from the adsorption isotherms for the single interface and for the thin film. This was done for a lipid film [17]. The free energy can also be evaluated by entropy theories [18]. These theories allow calculation of the decrease in the number of configurations of the adsorbed molecules due to steric hindrance. These two methods show that a repulsive force sufficient to stabilize the film is generated by a very small overlap of the chains of the two monolayers.

The problem is now to choose an analytical form for the repulsive forces, in order to be able to evaluate their role in a dynamic stability analysis of the black lipid films. Two different approaches were adopted:

3.1. The 'order parameter' approach [19]

An 'order parameter density' is introduced, describing the local concentration of oriented $-CH_2-$ monomers. In black films, the tails of the lipids belonging to adjacent surface layers hinder each

other so as to increase the order. This model gives rise to a stress contribution $\overline{\nabla}\cdot\overline{\overline{\Pi}}$ in the equation of motion (eq. 1), instead of the body force $\bar{F}_R$. Preliminary results of this model [19] are similar to those obtained here (see fig. 4 in section 5).

3.2. The 'repulsive body force' approach

In this approach, developed in the present paper, the repulsive interactions are introduced in eq. 1 as body forces, deriving from a repulsive potential $W_R(\bar{r})$. For constant fluid density in the three phases and negligible interactions in phases 1 and 3, this potential is given by:

$$W_R(\bar{r}) = \rho_2 \int_{V'} w_R(|\bar{r}-\bar{r}'|)\,d\bar{r}' \tag{11}$$

where V is the film volume. The equilibrium potential (superscript ^{eq}) is then given by:

$$W_R^{eq}(z) = \int_{-h/2}^{h/2} F(|z-z'|)\,dz' \tag{12}$$

where

$$F(|z-z'|) = \rho_2 \int_{|z-z'|}^{\infty} w_R(r)\,2\pi r\,dr \tag{13}$$

and h is the film width.

The steric potential energy per cm^2 film is defined by:

$$V_R^{eq}(h) = \frac{\rho_2}{2}\int_{-h/2}^{h/2} W_R^{eq}(z)\,dz. \tag{14}$$

Several hypotheses are used in obtaining eq. 14.

Hypothesis 1: the fluid density ρ_2 is supposed to be constant along the z-axis. This is a rather good approximation for the thinnest films, for which the volume fraction of oleate chains is nearly unity, except in the center of the film [11]. This assumption may fail for thicker films in which a greater amount of solvent is present.

Hypothesis 2: the fluid density takes into account globally the density of chains and solvent:

$$\rho_2 = \rho_2^{chains} + \rho_2^{solvent} = \text{constant}. \tag{15}$$

Discrepancies in stability results due to differences of solvent [11,12] cannot be accounted for by our treatment. In order to generalize the treatment to all kinds of solvents, a density $\rho_2(|\bar{r}-\bar{r}'|)$ should be used instead of ρ_2 in eq. 11.

The form of the potential $V_R^{eq}(h)$ can then be deduced from experimental curves for which the repulsive contribution to the free energy of formation of a film is measured. Such measurements have been made in detail for black films of glycerol monooleate in nonpolar solvents [11]. An electrical potential applied across the liquid film subjects it to a large compressive force under which most types of films become significantly thinner. From thickness measurements in an applied field, the strengths of the steric interactions which stabilize the film are calculated. From a knowledge of these steric interactions together with an estimate of the van der Waals forces from contact angle measurements, the curve of potential energy ΔA against film thickness can be calculated for the system, according to

$$\Delta A = \Delta A_V + \Delta A_R \tag{16}$$

where ΔA_V is the attractive van der Waals part of the free energy and ΔA_R the repulsive steric part. These components are shown in fig. 3. We made a fit of the repulsive part by an exponential form and identified it to $V_R^{eq}(h)$:

$$\Delta A_R = D'\cdot\exp(-Bh) \equiv V_R^{eq}(h). \tag{17}$$

Using eqs. 14 and 11, we deduce a plausible form of the point-point repulsive interaction potential:

$$w_R(|\bar{r}-\bar{r}'|) = D\cdot\exp(-B|\bar{r}-\bar{r}'|) \tag{18a}$$

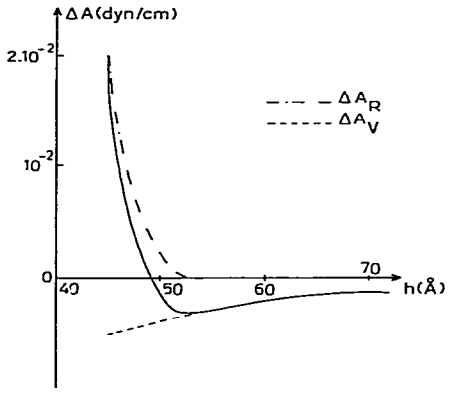

Fig. 3. Free energy change as a function of film thickness for glycerol monooleate + n-decane films in saturated NaCl. The dashed curves represent the separate van der Waals and steric interaction contributions (according to fig. 4 of ref. 11).

with

$$\frac{2\pi\rho_2^2 Dh}{B^3} = D'.$$

The form, eq. 18a, supposes that the point-point interaction is isotropic, and that the repulsive interactions are very small in fluids 1 and 3, compared to those in fluid 2 (D_1 and $D_3 \ll D$). We tested an alternative form,

$$w_R(|\bar{r} - \bar{r}'|) = D \cdot \exp(-B|z - z'|) \cdot \delta(x - x') \cdot \delta(y - y') \quad (18b)$$

which describes anisotropic repulsive interactions.

The parameters deduced from the fitting with the curves of fig. 3 are, respectively, $D' = 1.7 \times 10^{-4}$ dyn/cm and $B = 0.28$ (Å^{-1}) (or $1/B = 3.4$ Å). This corresponds to a very strong and rapidly decaying interaction, compared to the van der Waals interaction for the same case, i.e., $\Delta A_V(h) = -A/12\pi h^2$, with the Hamaker constant $A = 3.48 \times 10^{-14}$ erg.

In a first-order linear stability analysis, the perturbations of the steric interactions are expressed as for the van der Waals interactions in the jump of the pressure at each surface [1]:

$$\delta W_R = \frac{\partial W_R^0}{\partial z}\delta z + \delta W_R^1 \quad (19)$$

where δz is the perturbation of the surface coordinate. The first term on the right-hand side of eq. 19 is obtained by differentiating eq. 11 with respect to z at the reference flat state (superscript ^{0}) using eq. 18a. For interface s1, for instance, it is given by:

$$\left.\frac{\partial W_R^0}{\partial z}\right|_{s1} \delta z_{s1} = 2\pi\rho_2 Da\delta z_{s1} \quad (20)$$

with

$$a = \frac{-\exp(-Bh)}{B^2}(Bh + 1).$$

The second term of eq. 19 is the repulsive interaction at one surface due to the perturbation of the other surface, in the same way as was done for the van der Waals interactions [1].

For interface s1 it is given by (see appendix A):

$$\delta W_R^1|_{s1} = 2\pi\rho_2 Db(k)\delta z_{s2} \quad (21)$$

with

$$b(k) = \frac{Bh}{B^2 + k^2}\exp\left(-h\sqrt{B^2 + k^2}\right).$$

For long wavelengths ($k/B \ll 1$) the term $b(k)$ reduces to (l.w.l., long-wavelength limit):

$$\lim_{\text{l.w.l.}} b(k) = hB^{-1}\exp(-Bh)\left(1 - \left(\frac{k}{B}\right)^2 + \ldots\right) \quad (22)$$

By adding the two contributions, eqs. 20 and 21, the total perturbation (eq. 19) becomes, at surface s1

$$\delta W_R^1|_{s1} = 2\pi\rho_2 D[a\delta z_{s1} + b(k)\delta z_{s2}]. \quad (23)$$

and similarly at surface s2

$$\delta W_R^1|_{s2} = 2\pi\rho_2 D[a\delta z_{s2} + b(k)\delta z_{s1}].$$

The respective contributions of the repulsive forces to the BE and SQ modes will be discussed in section 5.

The alternative form (eq. 18b) gives more restricted results, i.e., $\bar{a} = -hB^{-1}\exp(-Bh)$ and $\bar{b} = hB^{-1}\exp(-Bh)$. These terms are independent of the wavelength so that they do not make any contributions to the BE mode. They will not be considered further.

4. The electrical contribution

In this section, we generalize the results already obtained [6] for the electrical interactions in a stability analysis.

Let us consider the general electrical potential profile of fig. 1b. The two monolayers display different electrical surface charges so that different electrical double layers extend outside in aqueous phases 1 and 3. Due to the difference in surface potential (α_{s1} and α_{s2}) or to an applied potential (ψ_0), a potential drop $\psi_m = \psi_0 + \alpha_{s1}^0 - \alpha_{s2}^0$ arises across the bilayer. This potential drop is supposed to be linear, due to the low dielectric constant of the lipid bilayer. The potential profile of fig. 1b is more general than the two separated profiles considered before [6] (equal surface charges or an applied field across a neutral membrane). In the reference state, we obtain for the electric fields in the three phases, respectively:

$$\left.\begin{aligned} E_1^0 &= -4\pi Z\Gamma_{s1}^0/\epsilon_1 = -\kappa_1\alpha_{s1}^0 \\ E_3^0 &= 4\pi Z\Gamma_{s2}^0/\epsilon_3 = \kappa_3\alpha_{s2}^0 \\ E_2^0 &= \psi_m/h \end{aligned}\right\} \quad (24)$$

where $Z\Gamma_{s1}^0$ and $Z\Gamma_{s2}^0$ are the surface charges, α_{s1}^0 and α_{s2}^0 the surface potentials, ϵ_1 and ϵ_3 the dielectric constants of solutions 1 and 3, κ_1 and κ_3 the inverse Debye lengths and ψ_m the potential drop across the film (transmembrane potential). As the aqueous solutions on both sides are similar, we suppose that $\epsilon_1 = \epsilon_3$ and $\kappa_1 = \kappa_3$.

When the surface is perturbed, the surface charge balance on each surface is required as additional boundary condition:

$$w\delta(Z\Gamma_s) = Z\Gamma_s^0 \frac{\partial v_z^s}{\partial z} + D_s k^2 \left[\delta(Z\Gamma_s) + \frac{Z^2\Gamma_s^0}{RT}\delta\alpha_s \right] + C\left[\delta(Z\Gamma_s) + \frac{Z^2\Gamma_s^0}{RT}\delta\alpha_s \right] \quad (25)$$

where v_z^s is the perturbed z-component of the surface velocity, $Z\Gamma_s$ the surface charge density, D_s the surface diffusion coefficient, C a chemical term which includes adsorption-desorption from the bulk phases or chemical reactions occurring at the surface, R the gas constant, T the absolute temperature, and $\delta\alpha_s$ the perturbation of the potential at the surface. The first term on the right-hand side of eq. 25 describes surface convection, the second surface diffusion-migration, and the third adsorption-desorption. Two limiting regimes can be considered here:

4.1. The fast regime ($w \gg k^2 D_s + C$)

In this case, the convection is fast compared to the two other processes. The perturbation of the surface charge (eq. 25) then reduces to the convection term

$$\delta(Z\Gamma_s) = Z\Gamma_s^0 \frac{\partial v_z^s}{\partial z} / w. \quad (26)$$

This regime has already been considered [6]. Moreover, we will suppose here that the surface charges remain constant during the perturbation, i.e., $\delta(Z\Gamma_s) = 0$.

4.2. The slow regime ($w \ll k^2 D_s + C$)

The convection is slow compared to the other processes. This regime adequately describes the surface dynamics of lipid films, for which the surface diffusion coefficient of the lipids is relatively high: $D_s = 1.5 \times 10^{-8}$ cm^2 s^{-1} [20].

If the charge variation does not depend on the area variation, we obtain by rearranging eq. 25:

$$\delta(Z\Gamma_s) = -\frac{Z^2\Gamma_s^0}{RT}\delta\alpha_s. \quad (27)$$

The variation of the surface charge is only dependent on the variation of the surface potential. For this case, we take the hypothesis of constant charge $\delta(Z\Gamma_s) = 0$ which corresponds to low surface charge $Z\Gamma^0/RT$, and the hypothesis of constant potential $\delta\alpha_s = 0$ which corresponds to high surface charge.

The relative contributions of the electrical terms to the two modes and to the coupling term are given in appendix B, for both regimes.

5. Results of a linear stability analysis

Asymptotic solutions of eq. 9 can be obtained in the long-wavelength limit ($kh \ll 1$, $k/B \ll 1$ and $k/k \ll 1$) and for viscosity $\mu \to 0$. The repulsive contributions are also taken in the long-wavelength limit (eq. 22), as well as the electrical contributions (appendix B). The van der Waals contribution is similar to those in previous studies [1,6].

Fluctuations with short characteristic lengths are not considered, since they are small in amplitude as a result of the large amounts of oil-water contact they would create and because of crowding of the lipid chains [12].

The marginal stability case ($w_R = w_i = 0$), for both fast and slow regimes, with the assumptions of constant charge or potential, is given by:

$$T_+(\mathrm{BE}) \cdot T_-(\mathrm{SQ}) - k^4(\mathrm{CO})^2 = 0 \quad (28a)$$

where

$$T_+(\mathrm{BE}) = k^2\left[\sigma_{s1}^0 + \sigma_{s2}^0 + \sigma_{s1}^E + \sigma_{s2}^E + \sigma_V + \sigma_R - \frac{\epsilon_2 h}{4\pi}\left(E_2^0\right)^2 \right] \quad (28b)$$

$$T_-(\mathrm{SQ}) = k^2\left[\sigma_{s1}^0 + \sigma_{s2}^0 + \sigma_{s1}^E + \sigma_{s2}^E \right] + \frac{4d\Pi_V}{dh} + \frac{4d\Pi_R}{dh} + \frac{4d\Pi_E}{dh} \quad (28c)$$

$$\mathrm{CO} = \left(\sigma_{s1}^0 - \sigma_{s2}^0\right) + \left(\sigma_{s1}^E - \sigma_{s2}^E\right). \quad (28d)$$

For the BE mode, the pure surface tensions σ_{s1}^0 and σ_{s2}^0 are the tensions of the monolayers on both sides of the Plateau border. The electrical surface

tensions due to the surface charges are given, in the long-wavelength limit, by:

$$\left.\begin{aligned}\sigma_{s1}^{E} &= -\frac{\epsilon_1}{8\pi\kappa_1}(E_1^0)^2 \\ \sigma_{s2}^{E} &= -\frac{\epsilon_1}{8\pi\kappa_1}(E_3^0)^2.\end{aligned}\right\} \tag{29}$$

The last term on the right-hand side of eq. 28b represents the electrical contribution to the surface tension due to the presence of an applied field E_2^0 in medium 2. Both electrical terms are negative and lower the pure surface tensions σ_{s1}^0 and σ_{s2}^0.

The van der Waals contribution to the surface tension in the long-wavelength limit is given by

$$\sigma_V = -\frac{3A}{12\pi h^2} \tag{30}$$

where $A = \pi^2\langle\rho_2^2\Lambda_{22} + \rho_1^2\Lambda_{11} - 2\rho_1\rho_2\Lambda_{12}\rangle$ is the Hamaker constant.

The repulsive contribution to the surface tension in the long-wavelength limit is given by

$$\sigma_R = D' \exp(-Bh) \equiv V_R^{eq}(h) \tag{31}$$

where D' and B are the parameters defined in eq. 18a. As $Bh \gg 1$, the factor 1 has been neglected in the expression of a (eq. 20).

The stability criterion for the uncoupled (BE) mode is [6]:

$$\sigma_F > 0 \text{ with } \sigma_F = \sigma_{s1}^0 + \sigma_{s2}^0 + \sigma_{s1}^E + \sigma_{s2}^E + \sigma_V + \sigma_R - \frac{\epsilon_2 h}{4\pi}(E_2^0)^2 \tag{32}$$

It can clearly be seen that the electrical and van der Waals interactions are destabilizing (they are negative, see eqs. 29 and 30), while repulsive steric interactions will stabilize the BE mode, especially when h decreases (this term is positive, see eq. 31).

For the SQ mode, the quantity

$$\frac{d\Pi_V}{dh} = -\frac{A}{2\pi h^4} \tag{33}$$

is the variation of the van der Waals disjoining pressure Π_V with respect to the film thickness. For $A > 0$, this quantity is negative and tends to decrease the term $k^2(\sigma_{s1}^0 + \sigma_{s2}^0)$ especially for long wavelengths.

The quantity

$$\frac{d\Pi_R}{dh} = D'B^2 \exp(-Bh) = \frac{d^2V_R^e}{dh^2} \tag{34}$$

is the variation of the repulsive disjoining pressure Π_R. This term is always positive, and expresses the overlap of the chains inside the film. The last term on the right-hand side of eq. 28c represents the variation of the electrical disjoining pressure Π_E. At the long-wavelength limit

$$\frac{d\Pi_E}{dh} = -\frac{\epsilon_2}{4\pi h^3}(E_2^0)^2. \tag{35}$$

The stability criterion for the uncoupled SQ mode is [6]:

$$k^2\sigma_F + 4\frac{d\Pi_F}{dh} > 0$$

which for the long-wavelength limit reduces to

$$\frac{d\Pi_F}{dh} > 0 \text{ with } \Pi_F = \Pi_V + \Pi_R + \Pi_E \tag{36}$$

By comparing the stability criteria for the BE mode (eq. 32) and SQ mode (eq. 36), it can clearly be seen that both take into account the film tension σ_F, but that for thickness fluctuations (SQ mode), there is a second component which describes the free energy of interaction between the two surfaces, and which is predominant at long wavelengths. The same result is obtained by an energy method [12], but using a global 'compressibility parameter' which does not specify the role of the different components.

For the coupling term, the asymmetry described by two different mechanical or electrical surface tensions leads to a new coupling between the BE and SQ modes, due to the differences in mechanical or electrical surface tension. This term has not been described before.

5.1. Stability for the uncoupled BE and SQ modes

Let us first discuss the membrane stability for the uncoupled BE and SQ modes, i.e., when the membrane is symmetric ($\sigma_{s1}^0 = \sigma_{s2}^0$). In order to compare with the experiments [11] on glycerol monooleate, we consider a neutral membrane ($\sigma_s^E = 0$ and $\psi_m = \psi_0$). In fig. 4, we plotted the neutral stability curve in the $h\psi_0$ plane, for the BE and SQ modes for long-wavelengths. The stability criteria (eqs. 32 and 36) indicate that the BE mode is unstable to the right of and above the solid curve $\sigma_F = 0$, while the SQ mode is unstable above the

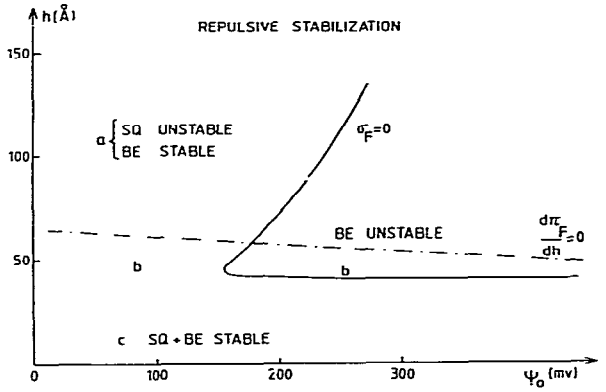

Fig. 4. Curves of marginal stability in the h-ψ_0 plane, for the BE mode ($\delta_F = 0$) and for the SQ mode ($d\Pi_F/dh = 0$).

dash-dotted curve $d\Pi_F/dh = 0$. Several regions of stability can be distinguished:

(Region a) For $h > 60$ Å, i.e., for colored films, the repulsive forces are not operative, the SQ mode is unstable while the BE mode is stable for most of the ψ_0 values.

(Region b) At $h \lesssim 60$ Å, the behavior changes fundamentally. As the two curves intersect each other, there is a region b, where at small potential ψ_0, both the BE mode and SQ mode are stable, while for a potential of about 160 mV, the film becomes unstable only with respect to BE mode fluctuations,

(Region c) For $h < 50$ Å, i.e., for black films, both the BE mode and sQ mode are stable for all ranges of potential ψ_0.

The parameters used to obtain fig. 4 are listed in table 1. They are deduced from experiments on glycerol monooleate films [11,12].

The main new result of fig. 4 is the stabilization of the SQ mode below $h \simeq 60$ Å, which is due to the steric repulsion of the hydrocarbon chains inside the film. This is in agreement with recent results [12], indicating that the preferred configuration of black lipid membranes is flat and that thickness fluctuations are small in amplitude. However, there is a range of thickness, 50 Å $< h <$ 60 Å, where the membrane thickness fluctuations are stabilized, while 'ripples' without thickness variations are still possible. This has important implications for the explanation of sinusoidal deformation of biological membranes (red blood cells [21]).

Table 1

Parameters for glycerol monooleate membranes

One-interface tension σ^0	0.5 dyn/cm
Membrane dielectric constant ϵ_2	2.0
Hamaker constant A	3.5×10^{-14} erg
Repulsive 'amplitude parameter' D'	1.7×10^{4} dyn/cm
Repulsive 'distance parameters' $1/B$	3.4 Å

5.2. Role of the asymmetry

The analysis of the dispersion relation with $W_R = W_i = 0$ provides a wavelength $(k_0)^{-1}$ which separates stable and unstable states. For unsymmetrical surface tensions (σ_s^0, σ_s^E), the two modes (BE and SQ) are coupled, and the system displays a marginal stability for a value of the dimensionless parameter $k_0 h$ obtained from eq. 28a:

$$(k_0 h) = \left[-\sigma_F h^2 (d\Pi_F/dh) \right]^{1/2} \times \left[\sigma_F (\sigma_{s1}^0 + \sigma_{s2}^0 + \sigma_{s1}^E + \sigma_{s2}^E + \sigma_V + \sigma_R) - (\sigma_{s1}^0 - \sigma_{s2}^0)^2 - (\sigma_{s1}^E - \sigma_{s2}^E)^2 \right]^{-1/2} \quad (37)$$

Eq. 28c shows that the stability of the SQ mode depends on the wavelength. This is not the case for the BE mode (eq. 28b). Therefore, eq. 37 may be compared with the marginal wavelength for the uncoupled SQ mode. From a mechanical point of view, this implies a symmetrical profile $\sigma_{s1}^0 = \sigma_{s2}^0$. From an electrical point a view, this can be obtained in two cases [6]:

(i) An electrical potential is applied on a neutral membrane (or with negligible surface charges $\sigma_{s1}^E = \sigma_{s2}^E \simeq 0$). The transmembrane potential ψ_m is equal in that case to the applied potential ($\psi_m = \psi_0$). Eq. 37 reduces to:

$$(k_0 h) = \left[\frac{-h^2 4(\Pi_V + \Pi_R + \Pi_E)/dh}{2\sigma_s^0 + \sigma_V + \sigma_R} \right]^{1/2} \quad (38)$$

(ii) The membrane has symmetrical surface charges $\sigma_{s1}^E = \sigma_{s2}^E$ and there is no applied field; eq. 37 becomes:

$$(k_0 h) = \left[\frac{-h^2 4(\Pi_V + \Pi_R) dh}{2\sigma_s^0 + 2\sigma_s^E + \sigma_V + \sigma_R} \right]^{1/2}. \quad (39)$$

We will focus on the comparison between the coupled unsymmetrical mode (eq. 37) and the uncoupled SQ mode (eq. 38 or 39), because this mode describes thickness variations of the membrane which may lead finally to membrane rupture. For that reason we choose parameters leading to a stable BE mode; according to the criterion, eq. 32, it means that $o_F > 0$.

In fig. 5a, we plotted the marginal curve obtained from eq. 38 for a pure SQ mode for negligible surface charges and for several values of an applied potential jump ψ_0 ($\psi_m = \psi_0$). The parameters are the same as in table 1, and we choose $h = 75$ Å so that the points representative of the parameters are situated in region a of fig. 4. Now the same potential jump inside the membrane can be obtained by modifying the surface charges on one side of a charged membrane. In that case, the two modes are coupled and we have plotted the marginal curve obtained from eq. 37 in fig. 5a; the

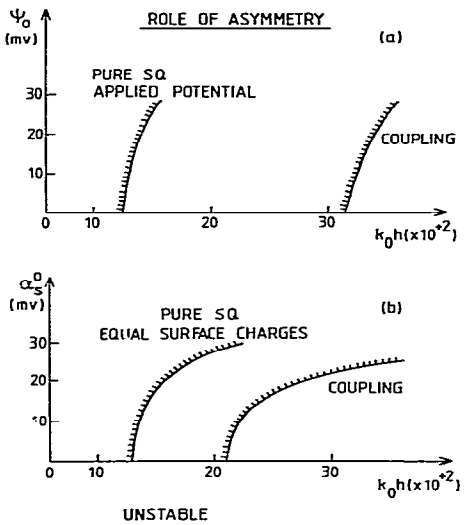

Fig. 5. (a) Curves of marginal stability as a function of the marginal wave number k_0 for a pure SQ mode and for coupled BE and SQ modes, in the case of an applied potential ψ_0 (negligible surface charges). (b) Curves of marginal stability for a pure SQ mode (equal surface charges or surface potential α_s^0) and for coupled BE and SQ modes (asymmetrical surface charges). The unstable regimes are on the dashed side of the marginal stability curves.

domain $k < k_0$ implies instability of the system, while for $k > k_0$, the system is stable. The coupling between the two modes leads to a larger unstable region, i.e., for a single value of ψ_0, an interval of wavelengths (a 'band') corresponds to unstable states for the coupled modes and to stable states for the uncoupled SQ mode. For both curves, as the applied potential ψ_0 increases, the unstable domain increases. This is due to the rise of the destabilizing electric term $d\Pi_E/dh$ compared to the constant value (fixed h and A) of the van der Waals and steric contributions.

In fig. 5b, we plotted the marginal stability curve (eq. 39) for pure SQ mode for several values of the surface potential α_s^0 in the case of a membrane with equal surface charges. The parameters are again listed in table 1, and σ_s^E is given by eq. 29 with $1/\kappa_1 = 1/\kappa_3 \simeq 10$ Å, which corresponds to electrolyte concentrations of about 0.2 M [22], and with dielectric constant of the solutions $\epsilon_1 = \epsilon_3 = 80$.

If the charge is modified on one side only, the two modes become coupled and it is clearly seen that the asymmetry induces a shift of the marginal stability curve to shorter wavelengths. The predictions of fig. 5b can be compared with experiments on asymmetric black lipid membranes [23]: bilayers composed of phosphatidylserine (PS) (charged lipids) are unstable under conditions of asymmetric distribution of Ca^{2+} or H^+ in the solution (0.1 M NaCl), i.e., on one side only, while these membranes remain stable with Ca^{2+} on both sides. In the framework of fig. 5b, these results can be qualitatively interpreted as follows: each PS molecule carries one negative charge at $6 < pH < 8$: this gives rise to a surface potential $\alpha_{s1}^0 = \alpha_{s2}^0 = \alpha_s^0$ (we are restricted in this treatment to small potentials $\leqslant 25$ mV), which in turn creates an electrical surface tension, due to the free energy of the diffuse double layers extending in the adjacent solutions. When Ca^{2+} is introduced on both sides of the membrane, it binds to the negative charges and reduces the surface potential from the same amount on both sides. The SQ mode remains stable for wavelengths situated to the right of the marginal stability curve. For example, for $\alpha_s^0 = 10$ mV and membrane width $h = 75$ Å, the marginal stability curve of fig. 5a predicts a stable system

for $(k_0 h) > 12.5 \times 10^{-2}$, i.e., for all wavelengths shorter than about 10^3 Å. When Ca^{2+} is introduced on one side only, this induces a change in electrical free energy on one side, and the two modes (BE and SQ) become coupled via the coupling term $(\sigma_{s1}^E - \sigma_{s2}^E)$. To proceed with the same example, for $\alpha_{s1}^0 \simeq 10$ mV on one side, the marginal curve of fig. 5b for the coupled situation predicts a shift to wavelengths half as long. This means that there is a 'band of wavelengths' between the two curves of fig. 5b for which the membrane will be destabilized by asymmetry. As this band lies beneath the range of the Teflon orifices (diameter $\simeq 10^4$ Å) in which the membranes are formed, this instability is plausible. Instability of the SQ mode or of the two coupled modes means, in our hydrodynamic model, that thickness fluctuations are amplified; it may be a necessary step leading to bilayer rupture or 'breakdown' [24].

When extrapolated to biological membranes, these results are in agreement with the 'bilayer couple' hypothesis [25], for which the two halves of the membrane bilayer are different and respond differently to various perturbations, while remaining coupled to one another (by van der Waals contact, for instance).

Finally, let us mention here thermodynamics studies on lipid bilayers (as an example, see ref. 26), based on the existence of lipid phase transitions. In fact, one striking feature of certain pure lipids and of mixtures of lipids is the appearance of supramolecular periodic structures observable in both freeze-fracture electron microscopy and X-ray diffraction. Theoretically, it can be shown [26] how a simple first-order chain-melting phase transition between a planar solid membrane and a planar fluid membrane is modified when the membrane has a spontaneous curvature. In addition, there is evidence that the two monolayer halves of the bilayer may be different or independent of one another, leading to a shift of the period of one monolayer relative to the other. Although derived from an equilibrium point of view, such studies provide support for the existence of dynamic modes BE and SQ and for the possibility of a coupling between them.

6. Conclusion

The method of linear stability analysis is applied to achieve a better understanding of the physical nature of the stability of a black lipid membrane. The hydrodynamic model consists of a thin lipid film considered as a Newtonian incompressible fluid, between two aqueous phases. Body forces (van der Waals, electrical and steric forces) are introduced in the equations of motion in the three phases.

Essentially, it is shown that the mode describing thickness variations (squeezing mode) is stabilized at small film thickness, due to the steric repulsion of the hydrocarbon chains inside the film. However, even a black lipid membrane can be destabilised by an asymmetric distribution of surface tensions or surface charges on the two sides of the film, in both fast and slow regimes. The dynamic model presented here and in previous publications comprises many of the essential features of lipidic films and provides a new insight into the dynamics of colored and black lipid films, and by extension of biological membranes.

Appendix A

The repulsive interaction at one interface s1 ($z = -h/2$) due to perturbation of the other interface $\tilde{h}/2$ is given by:

$$\delta W_R^1|_{s1} = \rho_2 D \int\int\int_{h/2}^{\tilde{h}/2} e^{-B(x^2+y^2+(\frac{h}{2}-z)^2)^{1/2}} \mathrm{d}x\,\mathrm{d}y\,\mathrm{d}z. \qquad \text{(A1)}$$

By expanding in a Taylor series around $h/2$, eq. A1 reduces to:

$$\delta W_R^1|_{s1} = \rho_2 D \delta z_{s2} \int\int e^{-i(k_x x + k_y y)} e^{-B(x^2+y^2+h^2)^{1/2}} \mathrm{d}x\,\mathrm{d}y. \qquad \text{(A2)}$$

After integration with respect to the y variable, eq. A2 becomes [27]

$$\delta W_R^1|_{s1} = 2\rho_2 D \delta z_{s2} \int e^{-ik_x x} K_1\left(B\sqrt{x^2+h^2}\right) \cdot \sqrt{x^2+h^2}\,\mathrm{d}x \qquad \text{(A3)}$$

where $K_1(z)$ is a modified Bessel function [28]. Integration of the real part of eq. A3 gives [27]:

$$\delta W_R^1|_{s1} = 4\rho_2 D \delta z_{s2} \sqrt{\frac{\Pi}{2}} \frac{B(h)^{3/2}}{(B^2+k^2)^{3/4}} K_{-3/2}\left(h\sqrt{B^2+k^2}\right). \qquad \text{(A4)}$$

For long wavelengths for which $k/B \ll 1$, we can evaluate the argument of the Bessel function by comparison with experiments [11]. Using the parameters $B \simeq 0.28$ Å^{-1} and $h \simeq 50$ Å we obtain $Bh \simeq 14$; the asymptotic form of the Bessel function can be used [28]:

$$K_{-3/2}\left(h\sqrt{B^2+k^2}\right) = \sqrt{\frac{\Pi}{2}}\,\frac{1}{(h)^{1/2}(B^2+k^2)^{1/4}}e^{-h\sqrt{B^2+k^2}} \times\left(1+\frac{1}{h\sqrt{B^2+k^2}}+\ldots\right) \quad \text{(A5)}$$

Replacing eq. A5 in eq. A4 we obtain

$$\delta W_{\mathrm{R}}^{1}|_{s1} = 2\Pi\rho_2 Db(k)\delta z_{s2}$$

$$\text{with } b(k) = \frac{Bh}{B^2+k^2}e^{-h\sqrt{B^2+k^2}}. \quad \text{(A6)}$$

Appendix B

The elements of the secular matrix (eq. 9) contain an electric part due to the Maxwell tensor (eq. 3), the (dis)continuity conditions and the conservation of surface charge (eq. 25).

For the fast regime, the secular determinant, for the electrical part, is given by:

	↤ ↤	↓ ↑	↤ ↦	↑ ↑
T_+	A_E	B_E	A_E^*	B_E^*
L_-	C_E	D_E	C_E	D_E^*
T_-	E_E^*	F_E^*	E_E	F_E
L_+	G_E^*	H_E^*	G_E	H_E

(B1)

We now give in detail the electrical terms for the fast regime and give their long-wavelength limit, in order to compare with previous results [6].

The electrical term A_E, which will make a contribution to be BE mode, is given by:

$$A_E = \frac{\epsilon_1(g-\kappa_1)(E_1^0+E_3^0)-\epsilon_1 g 2E_2^0}{4\pi D_1} \times\left[2\epsilon_2 kE_2^0\sinh(kh/2) + \epsilon_1(g-\kappa_1)(E_1^0+E_3^0)\cosh(kh/2)\right] + \frac{\epsilon_1(g-\kappa_1)(E_1^0-E_3^0)}{4\pi D_2}\epsilon_1(g-\kappa_1)(E_1^0-E_3^0)\sinh(kh/2) - \frac{1}{4\pi}\left[\epsilon_1(g-\kappa_1)E_1^0(E_1^0-E_2^0) + \epsilon_1(g-\kappa_1)E_3^0(E_3^0-E_2^0)\right]$$

with $g = \left(k^2+\kappa_1^2\right)^{1/2}$,

$D_1 = \epsilon_1 g_2\cosh(kh/2)+\epsilon_2 k\sinh(kh/2)$

and $D_2 = \epsilon_1 g_1\sinh(kh/2)+\epsilon_2 k\cosh(kh/2)$

which reduces in the long-wavelength limit (l.w.l.) ($k/g \ll 1$ and $kh \ll 1$) to

$$\lim_{\text{l.w.l.}} A_E = -\frac{\epsilon_1 k^2}{8\pi\kappa_1}(E_1^0)^2 - \frac{\epsilon_1 k^2}{8\pi\kappa_1}(E_3^0)^2 - \frac{2\epsilon_2 k^2 h}{8\pi}(E_2^0). \quad \text{(B2)}$$

Similarly, the electrical term E^{E}, which will make a contribution to the SQ mode, is given by:

$$E_E = \frac{\epsilon_1(g-\kappa_1)(E_1^0-E_3^0)}{4\pi D_1}\epsilon_1(g-\kappa_1)(E_1^0-E_3^0)\cosh(kh/2) + \frac{\epsilon_1(g-\kappa_1)(E_1^0+E_3^0)-2\epsilon_1 gE_2^0}{4\pi D_2} \times\left[2\epsilon_2 kE_2^0\cosh(kh/2) + \epsilon_1(g-\kappa_1)(E_1^0+E_3^0)\sinh(kh/2)\right] - \frac{1}{4\pi}\left[\epsilon_1(g-\kappa_1)E_1^0(E_1^0-E_2^0) + \epsilon_1(g-\kappa_1)E_3^0(E_3^0-E_2^0)\right]$$

which reduces in the long-wavelength limit to

$$\lim_{\text{l.w.l.}} E_E = -\frac{\epsilon_1 k^2}{8\pi\kappa_1}(E_1^0)^2 - \frac{\epsilon_1 k^2}{8\pi\kappa_1}(E_3^0)^2 - \frac{2\epsilon_2 k}{4\pi}(E_2^0)^2. \quad \text{(B3)}$$

The coupling term A_E^* (superscript * denotes a coupling term) is given by:

$$A_E^* = \frac{\epsilon_1(g-\kappa_1)(E_1^0-E_3^0)}{4\pi D_1} \times\left[2\epsilon_2 kE_2^0\sinh(kh/2)+\epsilon_1(g-\kappa_1)(E_1^0+E_3^0)\cosh(kh/2)\right] + \frac{\epsilon_1(g-\kappa_1)(E_1^0+E_3^0)-2\epsilon_1 gE_2^0}{4\pi D_2}\epsilon_1(g-\kappa_1) \times(E_1^0-E_3^0)\sinh(kh/2) - \frac{1}{4\pi}\left[\epsilon_1(g-\kappa_1)E_1^0(E_1^0-E_2^0) - \epsilon_1(g-\kappa_1)E_3^0(E_3^0-E_2^0)\right]$$

which reduces in the long-wavelength limit, to:

$$\lim_{\text{l.w.l.}} A_E^* = -\frac{\epsilon_1 k^2}{8\pi\kappa_1}(E_1^0)^2 + \frac{\epsilon_1 k^2}{8\pi\kappa_1}(E_3^0)^2 \quad \text{(B4)}$$

We obtain the same limit for the other coupling term, i.e.

$$\lim_{\text{l.w.l.}} E_E^* = \lim_{\text{l.w.l.}} A_E^*. \quad \text{(B5)}$$

The other terms corresponding to transversal displacements are zero in the long-wavelength limit, i.e.

$$\lim C_E = \lim G_E = \lim C_E^* = \lim G_E^* = 0.$$

The terms corresponding to longitudinal displacements are given by:

$$D_E = \frac{k^2}{4\pi D_1}\epsilon_1(E_1^0 + E_3^0)\cosh(kh/2)\left[2\epsilon_2 E_2^0 - \epsilon_1(E_1^0 + E_3^0)\right] - \frac{k^2\epsilon_1^2}{4\pi D_2}(E_3^0 - E_1^0)^2\sinh(kh/2). \quad \text{(B7)}$$

$$H_E = \frac{-k^2\epsilon_1^2}{4\pi D_1}(E_3^0 - E_1^0)^2\cosh(kh/2) + \frac{k^2}{4\pi D_2}E_1(E_1^0 + E_3^0)\sinh(kh/2) \times \left[-2\epsilon_2 E_2^0 + \epsilon_1(E_1^0 + E_3^0)\right]$$

$$D_E^* = \frac{k^2}{4\pi D_1}\epsilon_1(E_3^0 - E_1^0)\cosh(kh/2)\left[2\epsilon_2 E_2^0 - \epsilon_1(E_1^0 + E_3^0)\right] - \frac{k^2\epsilon_1^2}{4\pi D_2}\left[(E_3^0)^2 - (E_1^0)^2\right]\sinh(kh/2)$$

which reduces in the long-wavelength limit to

$$\lim D_E^* = \frac{k^2}{4\pi\kappa^*}\left[2\epsilon_2 E_2^0(E_3^0 - E_1^0) + 2\epsilon_1(E_1^0)^2 - 2\epsilon_1(E_3^0)^2\right]. \quad \text{(B9)}$$

We obtain the same limit for the other coupling term:

$$\lim H_E^* = \lim D_E^* \quad \text{(B10)}$$

The electric determinant reduces then in the long-wavelength limit to the expression

$$(A_E \times E_E) \times (D_E \times H_E) - (A_E^* \times D_E^*)^2. \quad \text{(B11)}$$

This expression describes the electrical coupling, due to the asymmetry, between the transversal parts of the BE mode and SQ mode, and the longitudinal parts of these modes.

In order to simplify the problem, we will suppose for the following that the charge remains constant during the perturbation, i.e., $\delta(Z\Gamma) = Z\Gamma^0\frac{\partial v_z}{\partial z}/w = 0$, which implies a low charge density $Z\Gamma^0$. Under that hypothesis, the determinant (eq. B1) reads

T	A_E	0	A_E^*	0
L	0	0	0	0
T	A_E^*	0	E_E	0
L	0	0	0	0

(B12)

which describes a coupling due to the asymmetry between the transversal parts of the BE mode and of the SQ mode. For the slow regime, under the simplifying assumptions given in section 4 (constant charge or constant potential), we obtain the same determinant (eq. B12) in the long-wavelength limit.

Acknowledgements

I wish to thank Dr. P.M. Bisch and Dr. H. Wendel for stimulating discussions in the earlier part of this work. Many colleagues provided constructive criticism of the manuscript, particularly M. Prevost, Dr. A. Steinchen and Professor A. Sanfeld. This research was supported by the Belgian Government (ARC 76/82 II.2).

References

1 B.U. Felderhof, J. Chem. Phys. 49 (1968) 44.
2 E. Ruckenstein and R.K. Jain, J. Chem. Soc. Faraday Trans. II, 70 (1974) 132.
3 A. Vrij, J.G.H. Joosten and H.M. Fijnaut, Adv. Chem. Phys. 68 (1981) 329 and references contained therein.
4. a. H.T. Tien, J. Gen. Physiol. 52 (1968) 125;
b. H.T. Tien, Bilayer lipid membranes (Marcel Dekker, New York, 1974);
c. H.T. Tien, in: Membranes and transport, ed. A.N. Martonosi (Plenum Press, New York, 1982) p. 165.
5 C. Maldarelli, R.K. Jain, I.B. Ivanov and E. Ruckenstein, J. Colloid Interface Sci. 78 (1981) 118.
6 H. Wendel, D. Gallez and P.M. Bisch, J. Colloid Interface Sci. 84 (1981) 1.
7 S.J. Singer and G.L. Nicolson, Science 175 (1972) 720.
8 P.M. Bisch, H. Wendel and D. Gallez, J. Colloid Interface Sci. 92 (1983) 105.
9 D. Gallez, P.M. Bisch and H. Wendel, J. Colloid Interface Sci. 92 (1983) 122.
10 A. Steinchen, D. Gallez and A. Sanfeld, J. Colloid Interface Sci. 85 (1982) 5.
11. D.M. Andrews, E.D. Manev and D.A. Haydon, Spec. Disc. Faraday Soc. 1 (1970) 46.
12 S.B. Hladky and D.W.R. Gruen, Biophys. J. 38 (1982) 251.
13 D. Bach and I.R. Miller, Biophys. J. 29 (1980) 183.
14 S. Chandrasekhar, Hydrodynamic and hydromagnetic stability (Oxford University Press, London, 1968).
15 D.N. Napper, J. Colloid Interface Sci. 58 (1977) 390.
16 R.H. Ottewill, in: Nonionic surfactants, ed. M.J. Schick (Marcel Dekker, New York, 1967) p. 649.
17 J.L. Taylor and D.A. Haydon, Disc. Faraday Soc. 42 (1966) 51.

18 E.J. Clayfield and E.C. Lumb, J. Colloid Interface Sci. 22 (1966) 269.
19 H. Wendel, P.M. Bisch and D. Gallez, Colloid Polymer Sci. 260 (1982) 425.
20 R.D. Kornberg and H.M. McConnell, Proc. Natl. Acad. Sci. U.S.A. 68 (1971) 2564.
21 W.T. Coakley and J.O.T. Deeley, Biochim. Biophys. Acta 602 (1980) 355.
22 H. Traüble, M. Teubner, P. Wolley and H. Eibl, Biophys. Chem. 4 (1976) 319.
23 D. Papahadjopoulos and S. Ohki, Science, 164 (1969) 1075.
24 Y.A. Chizmadzev, I.G. Abidor, V.F. Pastushev and V.B. Arakelya, Bioelectrochem. Bioenerg. 6 (1979) 37.
25 M.P. Sheetz and S.J. Singer, Proc. Natl. Acad. Sci. U.S.A. 71 (1974) 4457.
26 M.S. Falkovitz, M. Seul, H.L. Frisch and H. McConnell, Proc. Natl. Acad. Sci. U.S.A. 79 (1982) 3918.
27 I.S. Gradhsteyn and I.M. Ryzhik, Tables of integrals, series and products (Academic Press, New York, 1965).
28 M. Abramowitz and I.A. Segun, Handbook of mathematical functions (Dover, New York, 1965).